26

Extracellular Potassium Dynamics and Epileptogenesis

Flavio Fröhlich, Igor Timofeev, Terrence J. Sejnowski and Maxim Bazhenov

ABSTRACT

Extracellular ion concentrations change as a function of neuronal activity and represent important factors influencing the dynamic state of a population of neurons. In particular, relatively small changes in extracellular potassium concentration ($[K^+]_o$) mediate substantial changes in neuronal excitability and intrinsic firing patterns. While experimental approaches are limited in their ability to shed light on the dynamic feedback interaction between ion concentration and neural activity, computational models and dynamic system theory provide powerful tools to study activity-dependent modulation of intrinsic excitability mediated by extracellular ion concentration dynamics. In this chapter, we discuss the potential role of extracellular potassium concentration dynamics in the generation of epileptiform activity in neocortical networks. Detailed bifurcation analysis of a model pyramidal cell revealed a bistability with hysteresis between two distinct firing modes (tonic firing and slow bursting) for mildly elevated $[K^+]_o$. In neocortical network models, this bistability gives rise to previously unexplained slow alternating epochs of fast runs and slow bursting as recorded *in vivo* during neocortical electrographic seizures in cats and in human patients with the Lennox-Gastaut syndrome. We conclude that extracellular potassium concentration dynamics may play an important role in the generation of seizures.

INTRODUCTION

Epilepsy is one of the most common neurological disorders. Close to 5% of people in the world may have at least one seizure in their lifetime. At any time, 50 million people have epilepsy, especially in childhood, adolescence and old age. In developed countries, the annual incidence of epilepsy is estimated at 50 per 100 000 of the general population. Studies in developing countries, however, suggest that this figure is nearly double at 100 per 100 000 people. Up to 30% of people with epilepsy may not respond to pharmacological treatment (http://www.who.int/mediacentre/factsheets/fs165/en). These data illustrate that not enough is known about the mechanisms of epileptogenesis to treat it effectively. For the development of more effective antiepileptic drugs, it is therefore essential to better understand the underlying causes of the different forms of epileptic brain activity. Due to the complexity of neural dynamics, computational models with biological plausibility have become an important tool to study the epileptic brain.

While changes in the ionic composition of the extracellular milieu clearly modulate cortical network dynamics, experiments have only had limited success in providing a mechanistic understanding of ion concentration dynamics and epileptogenesis. In this chapter, we show how recent computational models of cortical circuits with extracellular potassium concentration ($[K+]_o$) dynamics help to overcome these previous limitations and contribute towards a more refined and experimentally testable theory of $[K+]_o$ dynamics and epilepsy. We first set the grounds by discussing the cortical origin of neocortical paroxysmal oscillations, *in vivo* and *in vitro* experiments concerning $[K+]_o$ dynamics, and the cortical network model with $[K+]_o$ dynamics. Then, we describe single cell dynamics including detailed bifurcation analysis of a novel bistability with hysteresis between tonic spiking and slow bursting mediated by $[K+]_o$. Next, we extend the model to the network level and describe mechanisms underlying slow state transitions between two distinct oscillatory firing modes (slow bursting and fast run). The transitions between episodes of slow bursting and fast run observed in the model exhibit the same qualitative features as those recorded *in vivo* during neocortical electrographic seizures in cat and in human patients with the Lennox-Gastaut syndrome. Then, we show mechanisms of seizure cessation. We conclude by discussing the novel insights derived from computational models and the potential implications for clinical research.

CORTICAL ORIGIN OF PAROXYSMAL OSCILLATIONS GENERATED WITHIN THE THALAMOCORTICAL SYSTEM

The origin of seizures that accompany various types of epileptic activities is unclear. Here we focus on neocortical seizures. The etiologies of epilepsies with cortical seizures include cortical dysplasia, traumatic injury and other idiopathic causes (Stafstrom, 2005). Anesthetized or naturally sleeping and awake cats exhibit seizures with transitions between periods of spike-wave complexes (2–3 Hz) and fast runs (10–15 Hz) (Steriade and Contreras, 1995; Steriade et al., 1998; Timofeev and Steriade, 2004). Similar transitions are observed in the electroencephalogram (EEG) of patients with the Lennox-Gastaut syndrome, a severe epileptic encephalopathy with neocortical seizures characterized by epochs of both slow spike or polyspike waves (SW/PSW) at 1.5–2.5 Hz and 10–20 Hz paroxysmal fast activity (Niedermeyer, 2002; Markand, 2003). Usually, the SW-PSW complexes of electrographic seizures correspond to clonic components of seizure, while the runs of fast spikes correspond to tonic components of seizures (Niedermeyer, 1999a,b).

Intracellular *in vivo* recordings reveal the physiology of neocortical seizures. During SW discharges, cortical neurons are depolarized and fire spikes during depth-negative (EEG spike) components and are hyperpolarized during depth-positive (EEG wave) components. A typical electrographic seizure consisting of SW-poly-SW (PSW) complexes recurring with frequencies of 1–3 Hz and fast runs with oscillation frequencies of 8–14 Hz is shown in Figure 26.1. The seizure starts with SW-PSW discharges. Epochs of fast run lasting several seconds interrupt the SW-PSW complexes. The seizure terminates with an epoch of SW discharges with decreasing frequency.

Recent experimental studies strongly suggest that both seizures with EEG pattern of the Lennox-Gastaut syndrome and spike-wave EEG complexes at around 3 Hz, as in petit-mal epilepsy, originate in neocortex (Pinault et al., 1998;

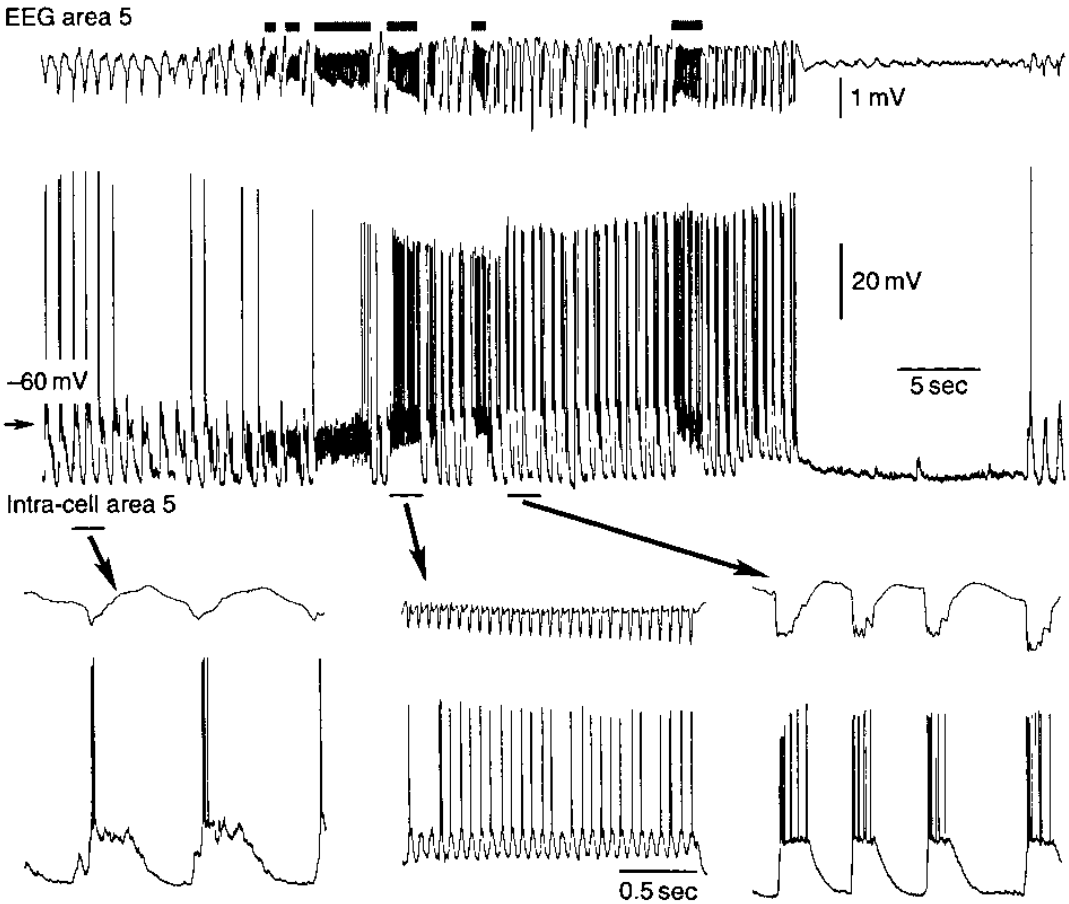

FIGURE 26.1 Electrographic seizure composed of spike-wave complexes and runs of fast paroxysmal spikes. Upper panel shows depth EEG and intracellular activity during normal slow oscillation and its transformation to paroxysmal activity composed of fast runs and spike-wave complexes. Thick gray lines indicate periods of fast runs. The other periods of the seizure are spike-wave complexes. Three expanded fragments indicated by horizontal bars and arrows show (from left to right) a period of slow oscillation, a paroxysmal fast run and a period of spike-wave discharges From Frohlich et al. (2006), with permission. Copyright 2006 Society for Neuroscience.

Steriade et al., 1998; Steriade and Contreras, 1998; Timofeev et al., 1998; Steriade, 2003; Timofeev and Steriade, 2004). The cortical origin is established by the following facts:

1. the presence of focal paroxysms both in neuronal pools within cortical depth (oscillations do not even reach the cortical surface (Steriade, 1974)) and in isolated cortical slabs *in vivo* (Timofeev et al., 1998)
2. the induction of neocortical seizures by infusion of the $GABA_A$-receptor antagonist bicuculline in neocortex of ipsilaterally thalamectomized cats (Steriade and Contreras, 1998)
3. the absence of SW seizures after intrathalamic injections of bicuculline *in vitro* (Bal et al., 1995) and *in vivo* (Ajmone-Marsan and Ralston, 1956; Steriade and Contreras, 1998; Castro-Alamancos, 1999)
4. hyperpolarization of the vast majority of thalamocortical (TC) neurons without action potentials during paroxysmal discharges recorded in corresponding cortical areas (Steriade and Contreras, 1995; Pinault et al., 1998; Timofeev et al., 1998; Steriade and Timofeev, 2001; Timofeev and Steriade, 2004).

Fast runs also originate in neocortex. Fast runs and spindles, which originate in thalamus, share similar frequencies and duration. This could suggest that both paroxysmal fast runs and spindles are caused by similar mechanisms and that therefore fast runs originate in the thalamus. However, experiments demonstrated that during fast runs:

1. TC neurons display excitatory postsynaptic potentials (EPSPs) that rarely lead to action potential generation (Timofeev et al., 1998)
2. no rebound Ca^{2+} spikes triggered by inhibitory postsynaptic potentials (IPSPs) occur
3. EPSPs in TC neurons follow cortical neurons, whereas the Ca^{2+} spike bursts in TC neurons precede cortical depolarizing potentials during spindles (see Figure 11 in Timofeev et al., 1998).

Furthermore, runs of fast paroxysmal EEG spikes were recorded in isolated neocortical slabs (Timofeev et al., 1998). In sum, these observations support the cortical origin of fast runs.

This section has summarized the substantial experimental evidence for the cortical origin of neocortical seizures both for spike-wave and for fast run episodes. In the next section, we discuss experimental evidence for the role of extracellular ion concentration dynamics in epileptogenesis.

CHANGES IN THE EXTRACELLULAR MILIEU AND EPILEPTOGENESIS

The role and significance of extracellular potassium concentration $[K+]_o$ dynamics in the central nervous system has been subject of considerable debate over the past decades. In this section, we summarize findings from both *in vivo* and *in vitro* experiments. We suggest that oversimplified assumptions and experimental difficulties have left most of the crucial questions about $[K+]_o$ dynamics and epileptogenesis unanswered. We conclude this section by explaining how detailed computational models of neural circuits and the interstitial space can provide clarifying insights into the role of $[K+]_o$ in epileptogenesis.

In vivo measurement with potassium-selective microelectrodes have established that $[K+]_o$ is modulated in an activity-dependent way. Visual stimulation and electrical activation of afferent pathways transiently increased $[K+]_o$ in cat lateral geniculate nucleus of the thalamus (Singer and Lux, 1973). Paired $[K+]_o$ and extracellular single unit recordings in cat striate cortex showed tight correlations (Singer and Lux, 1975). In cat somatosensory cortex, moving a brush across the contralateral forepaw increased $[K+]_o$ (Heinemann et al., 1977). A number of studies consistently showed that $[K+]_o$ changes dramatically during epileptic activity in cortex and spinal cord. Dual neuron-glia intracellular recordings from cortical suprasylvian association areas 5 and 7 of cats under ketamine-xylazine anesthesia revealed phasic negative events in glial membrane potential that were related to the onset of the paroxysmal depolarizing shifts in neurons (Amzica and Steriade, 2000). Although early studies used glia cell recordings and loading of the brain with radioactive labeled potassium (Grossman and Hampton, 1968; Fertziger and Ranck, 1970; Sypert and Ward, 1971; Dichter et al., 1972), later studies used potassium-selective microelectrodes (Lux and Neher, 1973) to show modulation of $[K+]_o$ during seizures and activity evoked by electrical stimulation in cortex (Hotson et al., 1973; Prince et al., 1973; Futamachi et al., 1974; Moody et al., 1974; Sypert and Ward, 1974; Lothman et al., 1975; Heinemann and Lux, 1977; Heinemann et al., 1977). Based on the measured increase in $[K+]_o$ during seizures, $[K+]_o$ was initially suggested to be the primary cause for both seizure initiation and termination (Fertziger and Ranck, 1970). According to this potassium accumulation hypothesis, an initial increase in $[K+]_o$ causes an increase in excitability which in turn further promotes $[K+]_o$ accumulation. Due to the

regenerative nature of this mechanism, $[K+]_o$ will eventually sufficiently increase to silence the neurons ('cathodal block') which will result in seizure termination.

Many other studies, however, found little evidence in support of the potassium accumulation hypothesis. Rather, in apparent contradiction to the potassium accumulation hypothesis, most *in vivo* studies reported an absence of a $[K+]_o$ threshold for seizure initiation (e.g. Futamachi et al., 1974), a delayed rise of $[K+]_o$ following a paroxysmal increase in neural firing (e.g. Heinemann et al., 1977) and a decrease in $[K+]_o$ during clonic phases of epileptic fits (e.g. Sypert and Ward, 1974). We propose that the rejection of the potassium accumulation hypothesis was mostly based on oversimplified assumptions and indirect conclusions. Specifically, a critical point for the initiation of the positive feedback loop between neural activity and increase in $[K+]_o$ can exist in absence of a unique, experimentally determinable threshold value since other factors are likely to modulate excitability. Therefore, the threshold value could differ from experiment to experiment. Moreover, a spatial mismatch between origin of the seizure and the potassium-selective microelectrode can further complicate the establishment of a causal link between $[K+]_o$ and epileptogenesis. Most importantly, the *in vivo* studies discussed above did not permit experiments which required the control of $[K+]_o$.

In contrast to the *in vivo* situation, the acute slice preparation provided the opportunity to at least partially control $[K+]_o$ and therefore to test more directly for a causal role between increase in $[K+]_o$ and epileptogensis. A series of studies, mostly in hippocampal slices, showed that an increase in $[K+]_o$ can indeed lead to various interictal and ictal phenomena. Here, we discuss a few examples illustrating some key insights from *in vitro* studies. A threshold in $[K+]_o$ for triggering non-synaptic paroxysmal events in hippocampus CA1 by locally applied K^+ and progressive increase in $[K+]_o$ before onset of a spontaneous seizure-like event suggest a causal role of $[K+]_o$ (Yaari et al., 1986). Spontaneous synaptic epileptiform activity with K^+-dependent frequency modulation occurred in CA3 hippocampal slice in elevated $[K+]_o$ (Rutecki et al., 1985). $[K+]_o$ increased during the tonic phase and decreased during the clonic phase of ictal events in hippocampal slices (Jensen and Yaari, 1997). CA1 pyramidal cells switched from tonic firing to bursting in response to depolarizing current injections when $[K+]_o$ was artificially increased (Jensen et al., 1994). However, although these studies suggest a potential causal role of $[K+]_o$ and provide important insight into cellular mechanisms, it is unclear how the observed phenomena translate to the intact brain.

Increase in extracellular $[K+]_o$ can potentially be a result of deficits in the potassium regulatory system. Indeed, hippocampal tissue from human patients with temporal lobe epilepsy exhibited impairment of glial inward-rectifying K^+-channels responsible for K^+ uptake (Hinterkeuser et al., 2000; Kivi et al., 2000). On the other hand, recordings in rat hippocampal slices revealed that the regulation of $[K+]_o$ is not impaired after injury and it was suggested that the larger $[K+]_o$ increase evoked by neuronal activity is a consequence, rather than the primary mechanism underlying post-traumatic hyperexcitability (Santhakumar et al., 2003).

Although it remains mostly unclear how the above-described limitations of *in vivo* and *in vitro* experiments can be overcome, recent computational models of cortical circuits and ion concentration dynamics in the interstitial space allow us for the first time to address crucial questions concerning how $[K+]_o$ shapes cortical dynamics. In this chapter, we summarize our results that address the role of $[K+]_o$ in mediating sustained oscillatory activity in the absence of external input. Although the original question about the causal role of $[K+]_o$ for seizure initiation remains unanswered for the time being, results from computational models illustrate that the initial hypothesis of a positive feedback mechanism leading to seizures by a global loss of stability (potassium accumulation hypothesis) needs substantial refinement. Specifically, our computational models reconcile intracellular recordings of neocortical seizure with the previously neglected findings that $[K+]_o$ increases during the tonic and decreases during the clonic phase both *in vivo* (Sypert and Ward, 1974) and *in vitro* (Jensen and Yaari, 1997) and that the firing pattern of pyramidal cells depends on $[K+]_o$ (Jensen et al., 1994).

MODEL DESCRIPTION

In order to investigate the interaction of extracellular potassium concentration $[K+]_o$ dynamics and the firing behavior of networks of cortical neurons, a computational network model of synaptically coupled cortical pyramidal cells and inhibitory interneurons was devised. In the model, each cell was surrounded by an extracellular compartment endowed with potassium concentration regulation mechanisms (Bazhenov et al., 2004; Frohlich et al., 2006). This section describes the computational model of individual cells, the synaptic coupling and the extracellular ion concentration dynamics.

SINGLE CELL MODEL

Each model neuron was endowed with both intrinsic and synaptic currents and consisted of an axo-somatic compartment with membrane voltage V_S described by

$$g(V_S - V_D) = -I_S^{int},$$

and a dendritic compartment with membrane voltage V_D with

$$C_m dV_D/dt = -g_L(V_D - E_L) - g(V_D - V_S) - I_D^{int} - I^{syn}$$

where g is the coupling conductance between the two compartments, I_S^{int} and I_D^{int} are the intrinsic currents in the respective compartments, C_m is the membrane capacitance, g_L and E_L are the conductance and reversal potential of the leak current, respectively (Mainen and Sejnowski, 1996; Frohlich and Bazhenov, 2006). The axo-somatic capacitance was approximated by zero for computational efficiency (Mainen and Sejnowski, 1996). The ratio of dendritic to axo-somatic surface area r was chosen to reproduce regular spiking ($r = 165$) and fast-spiking ($r = 50$) firing behavior for pyramidal cells (PYs) and inhibitory interneurons (INs), respectively. Intrinsic ionic currents were modeled with a set of Hodgkin-Huxley type conductances. Fast inactivating Na^+ channels (high and low density in axo-somatic and dendritic compartment, respectively) and fast delayed rectifier K^+ channels (axo-somatic compartment) mediated action potentials. Persistent sodium conductance G_{NaP}, slow voltage-gated K^+ conductance G_{Km}, slow calcium-activated K^+ conductance G_{KCa}, high-threshold Ca^{2+} conductance G_{Ca}, and hyperpolarization-activated depolarizing conductance G_h were included in the dendritic compartment and K^+ leak conductance G_L was introduced in both axo-somatic and dendritic compartments (Timofeev et al., 2000; Frohlich and Bazhenov, 2006).

SYNAPTIC DYNAMICS

Synaptic transmission was modeled by first-order kinetics of neurotransmitter binding and unbinding to postsynaptic receptors (Destexhe et al., 1994). With rectangular neurotransmitter concentration time-courses, the time-course of the fraction of open-receptors [O](t) after a presynaptic action potential equaled a single exponential. All synaptic currents I_{syn} were described by

$$I_{syn} = g_{syn}[O](V - E_{syn})$$

where g_{syn} is the maximal conductance (total synaptic conductances: $g_{AMPA(PY-PY)} = 0.15\,\mu S$, $g_{NMDA(PY-PY)} = 0.01\,\mu S$, $g_{AMPA(PY-IN)} = 0.07\,\mu S$, $g_{NMDA(PY-IN)} = 0.008\,\mu S$, $g_{GABA(IN-PY)} = 0.05\,\mu S$) and E_{syn} the reversal potential ($E_{AMPA} = 0\,mV$, $E_{NMDA} = 0\,mV$, $E_{GABA(A)} = -75\,mV$). Dependence of NMDA receptors on postsynaptic membrane voltage V_{post} was modeled by $1/(1 + \exp(-(V_{post} - V_{th})/\sigma))$ with $V_{th} = -25\,mV$ and $\sigma = 12.5\,mV$.

Excitatory synapses included short-term depression described by a depression variable $D \leq 1$ which was multiplied with the maximal synaptic conductance after each presynaptic spike (Tsodyks and Markram, 1997; Markram et al., 1998). D was adjusted with factor $R = 0.93$ (7% resources per action potential) from its previous value D_t after a presynaptic spike at time t_t with recovery time constant $\tau = 700\,ms$:

$$D = 1 - (1 - D_t R)\exp(-(t - t_t)/\tau).$$

The network dynamics discussed here resulted from the simulation of networks with various sizes. All networks, however, exhibited a similar structure consisting of a one-dimensional layer of pyramidal cells and a one-dimensional layer of inhibitory interneurons. In case of a very small network (e.g. 5 PYs and 1 IN), network connectivity was global, such that each cell projected to all other cells. Specifically, each PY cell was connected to every other PY cell by excitatory synapses (AMPA and NMDA). The IN received excitatory input from all PY cells (AMPA and NMDA) and inhibited all PY cells ($GABA_A$). For larger networks, the synaptic connectivity was local with synaptic footprints few neurons wide. For example, in the network model composed of two one-dimensional layers formed by 60 PYs and 15 INs respectively, each PY was connected to five neighboring PYs on either side, each PY excited three consecutive INs and each IN inhibited a total of eleven neighboring PYs. For all networks, the unitary conductance impinging on a given neuron was scaled by the total number of inputs.

POTASSIUM DYNAMICS

In the model, each neuron was surrounded by an extracellular compartment endowed with potassium regulation mechanisms. $[K+]_o$ was computed for both the dendritic ($[K+]_{o(D)}$) and the somatic compartment ($[K+]_{o(S)}$) of each cell. Processes affecting $[K+]_{o(D,S)}$ were channels permeable to K^+, K^+ pumps, glial K^+ uptake (buffering) G, and lateral diffusion current I_{Diff}:

$$d[K+]_{o(D,S)}/dt = (k/Fd)I_{\Sigma K} + G + I_{Diff(DS,SD)}$$

where $k = 10$ is a conversion factor, $F = 96489\,C/mol$ is the Faraday constant, and d is the ratio of the volume of the extracellular compartment to the surface area. The total potassium current $I_{\Sigma K}$ is the sum of all potassium currents (fast rectifying I_K, calcium-activated I_{KCa}, voltage-dependent non-inactivating I_{Km}, and leak current I_L) and the current I_{KPump} mediated by K^+ pumps:

$$I_{\Sigma K} = I_K + I_{KCa} + I_{Km} + I_L + I_{Kpump}$$

The K^+ pump current I_{KPump} was an inward current with a sigmoid dependence on the ratio of steady-state $[K+]_{o(eq)} = 3.5\,mM$ to current $[K+]_o$ and saturated at I_{max}, which was chosen to balance K^+ leak current (dendritic compartment $I_{max} = 5\,\mu A/cm^2$, somatic compartment $I_{max} = 40\,\mu A/cm^2$)

$$I_{KPump} = I_{max}/(1 + ([K+]_{o(cq)}/[K+]_o))^2.$$

Glial K^+ buffering current G was described by a free buffer (total buffer $[B_{max}] = 500\,mM$) with concentration [B], which bound and unbound from K^+ with according on- and off-rates $k_1 = 0.008$ and

$$k_2 = k_1/(1 + \exp(([K+]_o - [K+]_{o(th)})/-1.15))$$

governed by first order kinetics

$$d[B]/dt = k_1([B]_{max} - [B]) - k_2[K+]_o[B], \qquad G = k_1([B]_{max} - [B])/k_{1N} - k_2[K+]_o[B].$$

Threshold concentrations $[K+]_{o(th)}$ (15 mM for somatic compartment, 9 mM for dendritic compartment) and $k_{1N} = 1.1$ were chosen such that $[K+]_o$ equilibrated both for silent and for tonic firing mode (Bazhenov et al., 2004).

Diffusion currents between dendritic and axo-somatic compartments $I_{Diff(DS,SD)}$ were given by

$$I_{Diff(DS,SD)} = D([K+]_{o(D,S)} - [K+]_{o(S,D)})/\Delta x^2,$$

where $D = 4 \cdot 10^{-6}\,cm^2/s$ was the diffusion constant and $\Delta x = 100\,\mu m$ corresponded to the distance between the centers of the two compartments. In a subset of simulations, lateral diffusion between compartments corresponding to neighboring neurons was introduced

$$I_{Diff(lateral)} = D([K+]_{o(+)} - 2[K+]_o + [K+]_{o(-)})/\Delta x^2$$

where $[K+]_{o(+)}$ and $[K+]_{o(-)}$ represented the potassium concentration in the two neighboring compartments.

Any changes in $[K+]_o$ affected the reversal potential for all K^+ currents. The Nernst equation was used to compute the reversal potential for K^+ conductances

$$E_K = 26.64\,mV\ \ln([K+]_o/[K+]_i).$$

The reversal potential for G_h and G_L, both ion channels permeable to several ion types, were updated according to the Goldman-Hodgkin-Katz equation using the different ionic concentrations ($[Na^+]_o = 130\,mM$, $[Na^+]_i = 20\,mM$, $[Cl^-]_o = 130\,mM$, $[Cl^-]_i = 8\,mM$) and degrees of permeability:

$$E_h = 26.64\,mV\ \ln([K+]_o + 0.2[Na^+]_o)/([K+]_i + 0.2[Na^+]_i)$$

$$E_L = 26.64\,mV\ \ln([K+]_o + 0.085[Na^+]_o + 0.1[Cl^-]_i)/([K+]_i + 0.085[Na^+]_i + 0.1[Cl^-]_o).$$

SINGLE CELL DYNAMICS MEDIATED BY ELEVATED EXTRACELLULAR K^+

This section describes the dynamics of the above introduced model cortical pyramidal cell surrounded by an extracellular compartment endowed with potassium regulation mechanisms. We first describe the behavior of the model cell in response to a transient increase in extracellular K^+ concentration elicited by suprathreshold step depolarization. Then, we use bifurcation analysis to show the $[K+]_o$ dependence of the different firing patterns.

TRANSIENT OSCILLATION TRIGGERED BY INCREASE OF EXTRACELLULAR K^+ CONCENTRATION

The pyramidal cell (PY) model ($G_{Ca} = 0.022\,mS/cm^2$, $G_h = 0.1\,mS/cm^2$) showed oscillatory firing outlasting the stimulation with a suprathreshold DC pulse of 10 second duration (Figure 26.2A) (Timofeev et al., 2000; Bazhenov et al., 2004; Frohlich and Bazhenov, 2006; Frohlich et al., 2006). Directly after stimulation, the neuron fired bursts with a frequency of 2–3 Hz and a pronounced after-hyperpolarization at the end of each burst. After about 10 seconds of bursting, there was

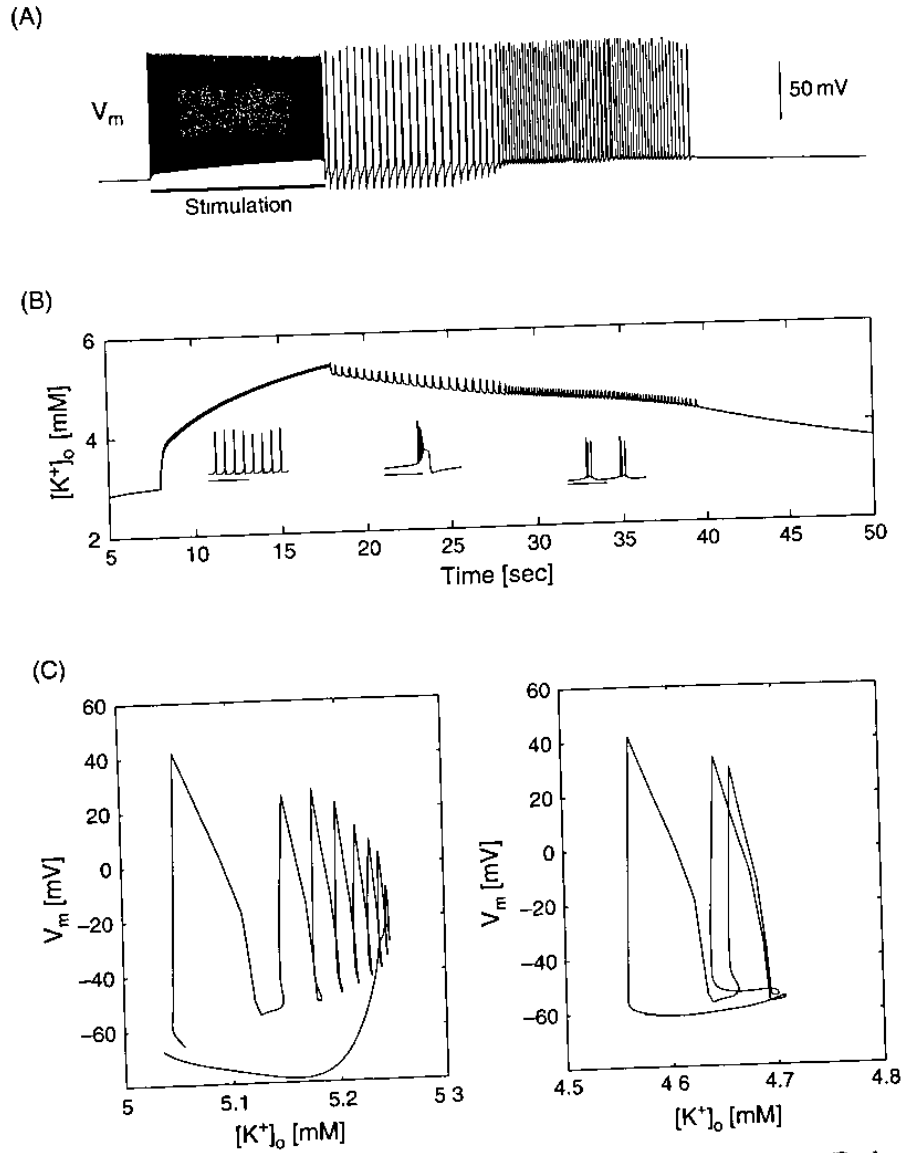

FIGURE 26.2 Single PY neuron stimulated with suprathreshold DC current pulse of 10 second duration (Bazhenov et al , 2004). (A) Membrane voltage time course The neuron exhibited high frequency firing during stimulation, switched first to bursting directly after stimulation (slow bursting, pronounced after hyperpolarization, duration about 10 seconds) and then to fast run (higher frequency, no after hyperpolarization, duration about 10 seconds) before returning back to its resting state. (B) Extracellular potassium concentration $[K+]_o$ increased during stimulation and gradually returned to baseline after stimulation. The insets illustrate the different oscillatory firing modes (calibration bars: 50 ms, 200 ms, 200 ms, respectively) (C) Phase plane plots showing membrane voltage as a function of $[K+]_o$ for slow bursting (left panel) and fast run (right panel)

a sharp transition to another oscillatory regime consisting of spike triplets at a higher frequency than the previous bursts. During this so-called fast run, no after-hyperpolarization was observed. About 10 seconds later, the neuron turned silent again and the membrane voltage eventually returned to the resting potential before stimulation.

During initial stimulation, the high frequency firing of the neuron (see Figure 26.2B, left inset) caused an increase in $[K+]_o$. In this condition, active and passive mechanisms decreasing the excess potassium were not sufficient to keep the potassium concentration near steady-state level. After stimulation, $[K+]_o$ decreased during both bursting (see Figure 26.2B, middle inset) and fast run (see Figure 26.2B, right inset) until it reached baseline again. Potassium efflux was mainly mediated by the fast delayed-rectifier (41% and 43% for bursting and fast run, respectively) and the leak conductance (43% and 56%, respectively). Each burst was accompanied by a noticeable change in $[K+]_o$ (see Figure 26.2C, left panel). In fast run, $[K+]_o$ changed only marginally during a triplet of spikes (see Figure 26.2C, right panel). This model of an isolated single cell surrounded by a spatially limited extracellular compartment showed that the cell was in different firing regimes as a function of $[K+]_o$. Since there was no K^+ diffusion, increase in $[K+]_o$ may be stronger and longer lasting in this model than *in vitro* or *in vivo*. To investigate how these transitions between silent state, bursting mode and fast run depend on $[K+]_o$, the K^+ regulation mechanism was switched off and $[K+]_o$ was treated as a constant (bifurcation analysis).

CO-EXISTENCE OF SLOW BURSTING AND TONIC FIRING

In this section, we treat $[K+]_o$ as a parameter to determine the firing behavior of the cell as a function of $[K+]_o$. Therefore, all mechanisms controlling $[K+]_o$ evolution in the model were blocked and the firing behavior was analyzed for different fixed values of $[K+]_o$ within the physiological range (Frohlich et al., 2006). Specifically, we focused on the occurrence of different stable firing modes as a function of parameter $[K+]_o$.

First, we discuss the stable fixed points of the system. For very low $[K+]_o$, the neuron was at rest. For increasing $[K+]_o$, the resting potential became more depolarized as the driving force for potassium decreased. For $[K+]_o = 4.85\,\text{mM}$, the silent state lost stability by means of a saddle-node bifurcation (Type I neural oscillator (Rinzel and Ermentrout, 1989; Ermentrout, 1996), fixed point bifurcations in Figure 26.3A). At $[K+]_o = 9.46\,\text{mM}$, a new stable state corresponding to a depolarized state with spike inactivation ($V_m = -26.3\,\text{mV}$) appeared by means of a subcritical Andronov-Hopf bifurcation (Figure 26.3A).

In order to characterize further the transition between tonic firing and slow bursting, we computed a Poincaré cross-section by calculating the values of intracellular calcium concentration $[Ca^{2+}]_i$ each time the membrane potential crossed the threshold $V_m = -20\,\text{mV}$; these values were plotted as a function of $[K+]_o$ (see Figure 26.3B). In such a representation, periodic oscillations (corresponding to limit cycles) are represented as points defined by a threshold crossing of a trajectory. This approach allows the graphical representation of changes in the nature of an oscillatory (firing) behavior as a function of a parameter. For a given value of $[K+]_o$, tonic spiking is represented by a single point on this Poincaré cross-section since $[Ca^{2+}]_i$ assumes the same value at $V_m = -20\,\text{mV}$ for every spike. During a burst, however, $[Ca^{2+}]_i$ increases after each spike of a given burst. Therefore, a burst appears as a vertical group of points each representing a single spike. In other words, a set of parallel horizontal lines in the Poincaré cross-section (see Figure 26.3B) delimits a range of $[K+]_o$ values for which bursting occurs.

For determining the Poincaré cross-section, $[K+]_o$ was gradually increased and decreased to reveal the complete tonic firing and slow bursting region, respectively. We found a bistability between tonic firing and slow bursting, which was associated with a hysteresis (evident by comparison of top and bottom plots in Figure 26.3B). For increasing $[K+]_o$, the cell stayed in tonic firing until slow bursting with spike inactivation became the only stable state at $[K+]_o = 6.40\,\text{mM}$. Decreasing $[K+]_o$ caused the cell to stay in slow bursting mode until tonic firing was the only stable state at $[K+]_o = 5.75\,\text{mM}$. For increasing $[K+]_o$ (see Figure 26.3B, top), the tonic firing region consisted of three subregions with single spikes, spike doublets and single spikes, respectively. Note that the left region with single spikes existed only in the case of a non-zero hyperpolarization-activated depolarizing conductance ($G_h = 0.05\,\text{mS/cm}^2$). For decreasing $[K+]_o$ (see Figure 26.3B, bottom) two distinct bursting regimes – with and without spike inactivation – were found (see Figure 26.3C).

MECHANISM OF BURST GENERATION

To study the bursting dynamics in the model, we used fast-slow analysis by choosing a state variable with dynamics on the time-scale of individual bursts in the complete system and treating it as a parameter of the resulting reduced system for a fixed value of $[K+]_o$ (Frohlich and Bazhenov, 2006). Here, the calcium-activated potassium conductance g_{KCa}, with a time scale at least as slow as the slow $[Ca^{2+}]_i$ dynamics, was chosen as the slow variable. The conductance g_{KCa}

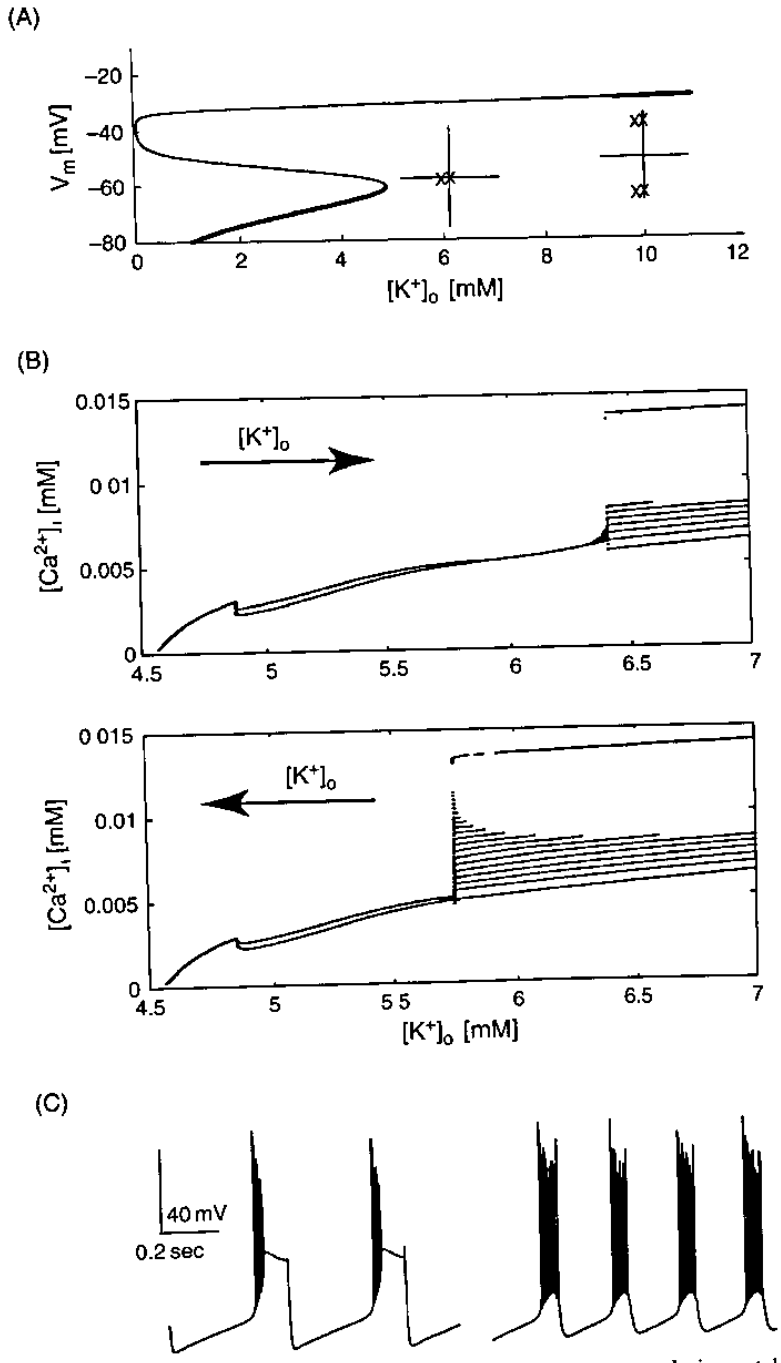

FIGURE 26.3 (A) Stable fix points corresponding to rest and the depolarized state are connected via unstable fix points. Transition from silent to tonic firing is a saddle-node bifurcation. Transition from slow bursting to depolarized is a Andronov-Hopf bifurcation. Insets illustrate eigenvalues at bifurcation points. (B) Poincaré cross-section for gradually increasing (top) and decreasing (bottom) $[K+]_o$. Tonic firing corresponds to a single point, spike doublets to two points and bursting to a series of points in the Poincaré cross-section for a given value of $[K+]_o$. Bistability between tonic firing and bursting for $[K+]_o$ between 5 75 and 6.4 mM. (C) Left. bursting with spike inactivation for $[K+]_o = 6.00$ mM (slow bursting branch, $[K+]_o$ decreasing). Right bursting without spike inactivation for $[K+]_o = 5.75$ mM (slow bursting branch, $[K+]_o$ decreasing) Adapted from Frohlich et al. (2006), with permission. Copyright 2006 Society for Neuroscience.

terminates bursts after sufficient calcium influx via the high-threshold calcium conductance, which was activated during the depolarized membrane state of each burst.

We here consider the case of $[K+]_o = 5.9$ mM which is within the bistable region (see Figure 26.3B). Although a conductance reflecting an assembly of ion channels cannot be negative, we included $g_{KCa} < 0$ to capture the entire bifurcation structure of the system. The bifurcation plot in Figure 26.4 shows the dendritic membrane voltage values that correspond to fixed points of the reduced system as a function of g_{KCa}. Similarly, for all limit cycles, maximum and minimum dendritic membrane voltages of the oscillatory trajectory are plotted. The fixed points of the reduced system follow a z-shaped line as a function of g_{KCa} (Figure 26.4, top panels). The two arms of stable fixed points, P^d_s and

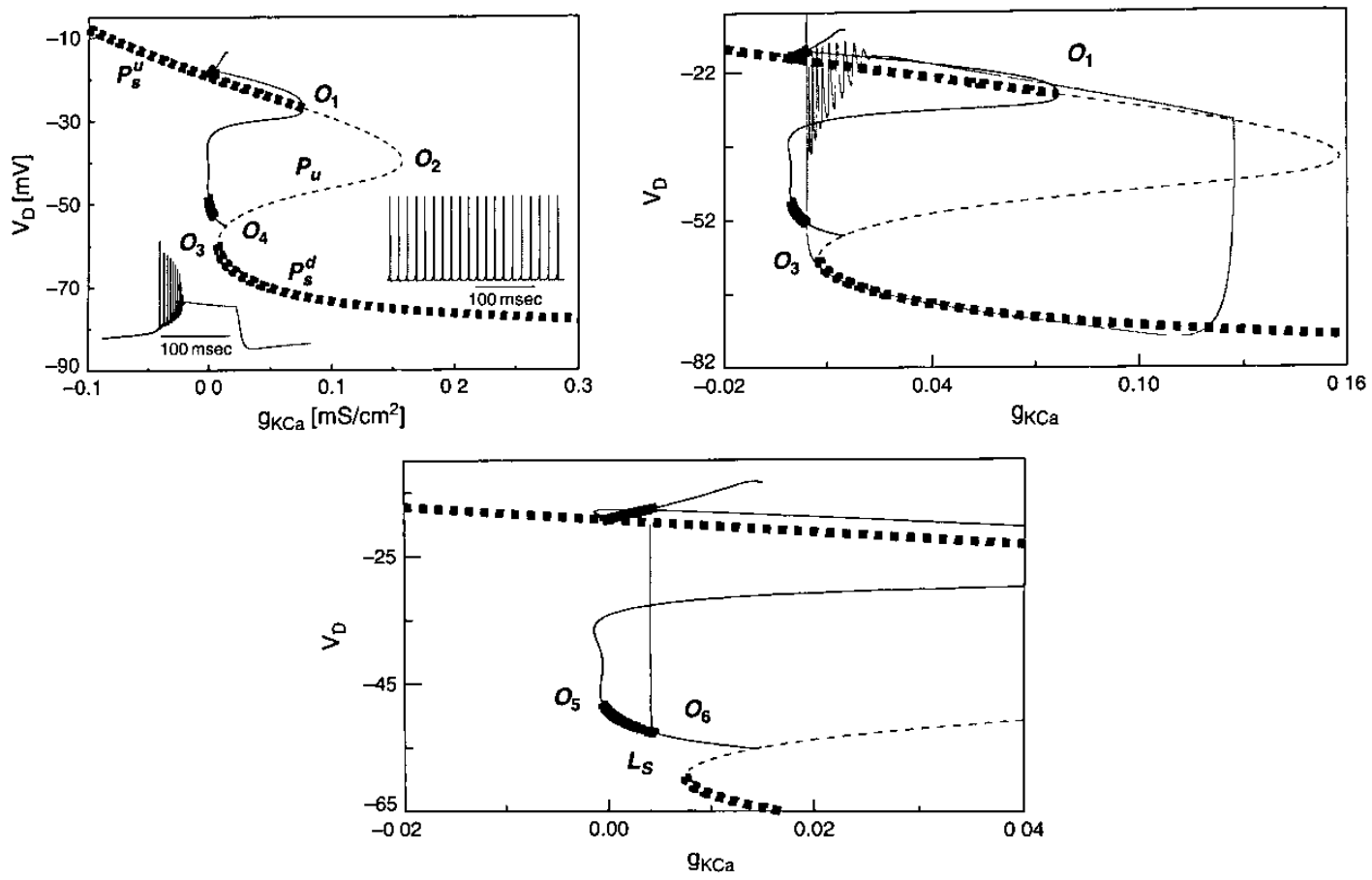

FIGURE 26.4 Bifurcation diagram of the reduced system for $[K+]_o = 5.9$ mM. Top left panel: Stable fixed points P^u_s and P^d_s (thick dashed line) are connected by the branch of unstable fixed points P_u (thin dashed line). Solid lines indicate stable (thick) and unstable (thin) limit cycles. O_1 Andronov-Hopf; O_2 and O_3, fold; O_4, saddle homoclinic orbit bifurcation points. Insets show bursting and tonic spiking patterns in the complete system with freely running g_{KCa} Top right and bottom panels: enlarged region of interest. O_5, Neimark-Sacker and O_6, period doubling bifurcation points. L_s indicates stable limit cycles Projection of the phase trajectory for the complete system during bursting mode (solid line, middle panel) and tonic firing (solid vertical line, bottom panel). Adapted from Frohlich and Bazhenov, (2006), with permission. Copyright 2006 by the American Physical Society.

P^u_s, are connected by a branch of unstable fixed points. Importantly, for g_{KCa} between 0.007 and 0.076 mS/cm^2, both stable states coexist. P^u_s loses stability by a subcritical Andronov-Hopf bifurcation at O_1. P^d_s coalesces with the unstable fixed point in a saddle-node bifurcation at O_3. In the following, we explain how this bifurcation landscape of fixed points in the reduced system explains the oscillatory bursting behavior in the complete system (Figure 26.4, top left panel).

During the hyperpolarized phase in between bursts, the system follows P^d_s and conductance g_{KCa} decreases since calcium removal mechanisms reduce intracellular calcium concentration. Eventually, P^d_s loses stability at the saddle-node bifurcation point O_3 causing a transition into the basin of attraction of P^u_s. The trajectory rotates several times around the stable focus P^u_s, but never quite reaches it. The rapid sequence of action potentials at the onset of burst is mediated by the trajectory approaching the stable fixed point. The decaying amplitude of the transient oscillations corresponds to the decreasing spike amplitude in the membrane voltage time-course during a burst. As the system approaches P^u_s, no more action potentials occur and the membrane voltage remains depolarized. In this depolarized state with spike inactivation, intracellular Ca^{2+} concentration increases due to the activation of the high-threshold Ca^{2+} conductance which mediates calcium influx. As a consequence, g_{KCa} increases which eventually leads to a loss of stability of P^u_s at O_1, forcing the trajectory back to P^d_s. In summary, bursting in the complete system corresponds to periodic transitions between two stable fixed points in the reduced system (point-point bursting mechanism (Izhikevich, 2007)).

MECHANISM OF TONIC SPIKING

In the previous section, we discussed the bifurcation landscape responsible for burst generation. We now turn our attention to tonic firing (see Figure 26.4, bottom panel). In the bifurcation diagram of the reduced model, tonic spiking corresponds to a limit cycle. Stability of the limit cycle in the reduced system is therefore necessary for occurrence of tonic firing. Whether tonic firing is stable in the full model depends on the value of g_{KCa} for which the limit cycle is stable in the

reduced system. Specifically, the value of g_{KCa} needs to be such that the corresponding intracellular calcium concentration can be achieved and maintained during tonic firing. Here, the bifurcations of the limit cycles in the reduced model are analyzed (again for $[K+]_o = 5.9\,mM$). In the bifurcation plot, the small-amplitude unstable limit cycle which arises at O_1 folds around at $g_{KCa} = -0.001\,mS/cm^2$ leading to the coexistence of a small- and a large-amplitude unstable limit cycle. Before merging with the unstable fixed point P_u in a saddle homoclinic orbit bifurcation at point O_4, the unstable limit cycle with larger amplitude in the V_D dimension becomes stable in a narrow range of g_{KCa} between -0.0005 and $0.0045\,mS/cm^2$. This stable region is delimited by a subcritical Neimark-Sacker bifurcation on the lower end (bifurcation point O_5) and a period-doubling bifurcation on the upper end (bifurcation point O_6). In the complete system, g_{KCa} is small during tonic firing since g_{Ca}, which causes calcium influx, is in average only weakly activated. Also, g_{KCa} is bounded by zero on the left side since an ionic conductance cannot become negative. Therefore, g_{KCa} is sufficiently constrained in the full system to fit the window of values for which a stable limit cycle was found in the reduced system. This limit cycle mediating tonic spiking dynamics coexists with the previously discussed periodic orbit mediating bursting. Therefore, the complete model of a cortical pyramidal cell exhibits bistability between slow bursting and tonic firing for elevated $[K+]_o$.

For values of $[K+]_o$ outside the region of hysteresis, the complete system displayed only tonic spiking or bursting dynamics (see Figure 26.3B). Bifurcation analysis for low values of $[K+]_o < 5.75\,mM$ revealed that the vicinity of the saddle-node point O_3 (see Figure 26.4, top left panel) no longer belongs to the basin of attraction of the upper stable fixed point P^u_s (Frohlich and Bazhenov, 2006). Therefore, for initial conditions on the low stable branch of fixed points P^d_s, the system reaches the saddle-node bifurcation point and moves to the stable limit cycle, mediating firing with spike doublets. Conversely, for high values of $[K+]_o > 6.4\,mM$, only bursting is stable in the complete system. The limit cycle corresponding to tonic spiking was found in the reduced system with g_{KCa}, however, it became unstable in the complete system (Frohlich and Bazhenov, 2006). Hence, tonic firing does not exist as a stable state for sufficiently elevated $[K+]_o$.

NETWORK DYNAMICS MEDIATED BY ELEVATED EXTRACELLULAR K^+

In the previous sections, we have presented an in-depth analysis of the model of a single cortical pyramidal cell surrounded by an extracellular compartment with potassium concentration dynamics. The bistability with hysteresis between tonic firing and slow bursting did not affect the spiking activity of a single pyramidal cell challenged by an increase in $[K+]_o$ since in either of the two firing regimes $[K+]_o$ decreased and only transient oscillations occurred. This is different in case of a network of neurons with $[K+]_o$ dynamics as we will show in this section.

SLOW STATE TRANSITIONS

In the single cell model, the after-discharge following stimulation was of finite length since $[K+]_o$ eventually returned to its baseline value. Here, we now discuss the slow dynamics in case of model cells interconnected with synapses to form cortical network models. First, we analyze the behavior of a small compact network which consists of five pyramidal cells (PYs) and one inhibitory interneuron (IN) with global connectivity. Such a small circuit is a direct extension of the single cell model due to its compact nature. Second, we show that our findings generalize to larger networks with more localized synaptic connectivity patterns. These larger networks exhibited not only very similar temporal dynamics but, additionally, also spatial patterning of the oscillatory activity.

Key difference between the single cell and the small network case is the duration of the K^+ mediated oscillatory dynamics. In case of a single cell, the transient firing exhibits patterning into two distinct epochs (slow bursting and fast run) before returning to the silent state. Conversely, in case of the network, we found indefinitely lasting oscillatory dynamics patterned into epochs of slow bursting and fast run. The slow state transitions between the two oscillatory modes occurred on the time-scale of seconds. Essentially, the slow dynamics are mediated by the above discussed bistability between tonic firing and slow bursting, which is maintained in the network model (Figure 26.5A). Specifically, bifurcation analysis for the network revealed a similar structure of $[K+]_o$ dependent firing modes (silence, fast run, slow bursting, depolarized locked state) exhibiting bistability with hysteresis for transitions between the different oscillatory firing types. In contrast to the single cell, however, $[K+]_o$ increased during fast run in the complete model with $[K+]_o$ as a dynamics variable. This key difference is responsible for the persistent nature of the oscillatory firing in the network model. While the cells were in fast run, $[K+]_o$ increased up to the level where fast run loses stability and the cells were forced to switch to slow bursting (upper end point of hysteresis). During slow bursting, however, $[K+]_o$ decreased. Because of the bistability with hysteresis, the cells stayed in slow bursting until the lower endpoint of the hysteresis was reached where the slow bursting mode loses stability and is replaced by fast run.

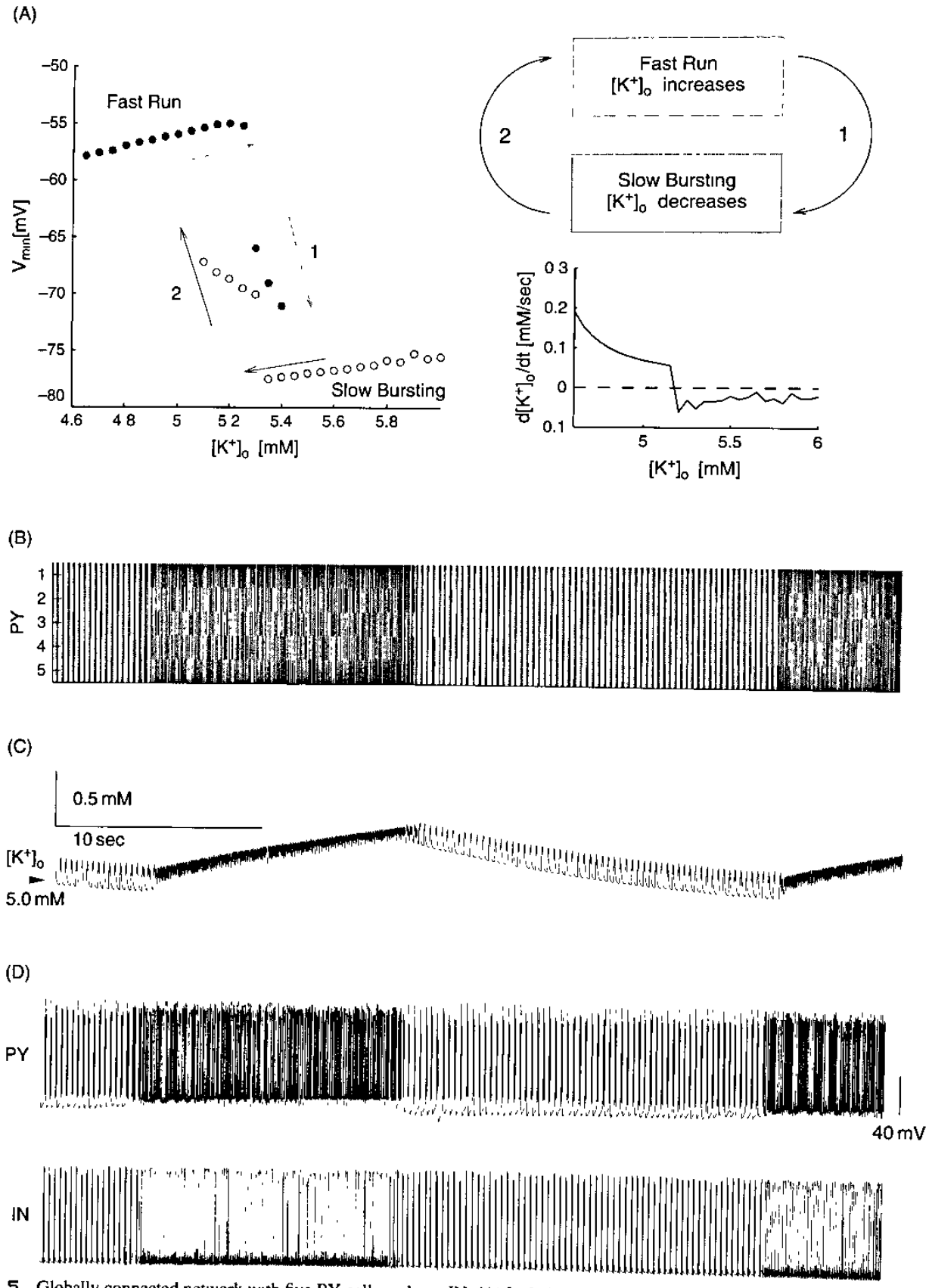

FIGURE 26.5 Globally connected network with five PY cells and one IN. (A) Left: bifurcation analysis (minimum of membrane voltage): hysteresis between fast run and slow bursting for $[K+]_o$ between 5.0 and 5.4 mM. Circles denote stable limit cycle oscillations. Top right: schematic of slow periodic network dynamics Bottom right, averaged $[K+]_o$ gradient as a function of $[K+]_o$. (B–D) Slow transitions after initial brief increase in $[K+]_o$ (B) Network activity of PY cells (40 seconds duration) shows alternating epochs of fast run and slow bursting. (C) $[K+]_o$ increased during fast run and decreased during slow bursting. Upper switching point for transition from fast run to slow bursting and lower switching point for transition from slow bursting to fast run correspond to hysteresis endpoints in (A). (D) Membrane voltage time course of PY cell (top trace) and of IN (bottom trace). From Frohlich et al. (2006), with permission Copyright 2006 Society for Neuroscience.

At this point, the network has gone through an epoch of fast run followed by an epoch of slow bursting (Figure 26.5B). The nature of the hysteresis forces the network to stay in the bistable region leading to an infinite sequence of such alternating epochs of slow bursting and fast run (Figure 26.5C,D).

Since the network connectivity was found to be critical for the slow state transitions to occur, simulations for a range of excitatory and inhibitory coupling strengths were used to determine the conditions that the synaptic coupling strengths need to fulfill for the slow state transitions to occur. Simulations sampling all pairs of excitatory (lateral recurrent excitation) and inhibitory (inhibition mediated by interneurons) coupling strengths for a range of 80% to 120% of the original values used in the model revealed that the occurrence of slow state transitions is a robust phenomenon at a broad range of coupling strengths, as long as synaptic excitation and inhibition are scaled such that the balance between excitation and inhibition is maintained (Figure 26.6). An unbalanced increase in excitation favored the occurrence of slow bursting, resulting in an increase in the duration of slow bursting epochs and an increase in the width of the hysteresis between slow bursting and fast run (Figure 26.6A). The latter phenomenon was caused by a lowering of the $[K+]_o$ threshold for which the network switched from slow bursting to fast run (lower endpoint of hysteresis, Figure 26.6B). Conversely, an unbalanced increase in synaptic inhibition caused an increase in the duration of the epochs of fast run by narrowing the width of hysteresis through increase of $[K+]_o$ threshold for transition from slow bursting to fast run (lower endpoint of hysteresis). In cases

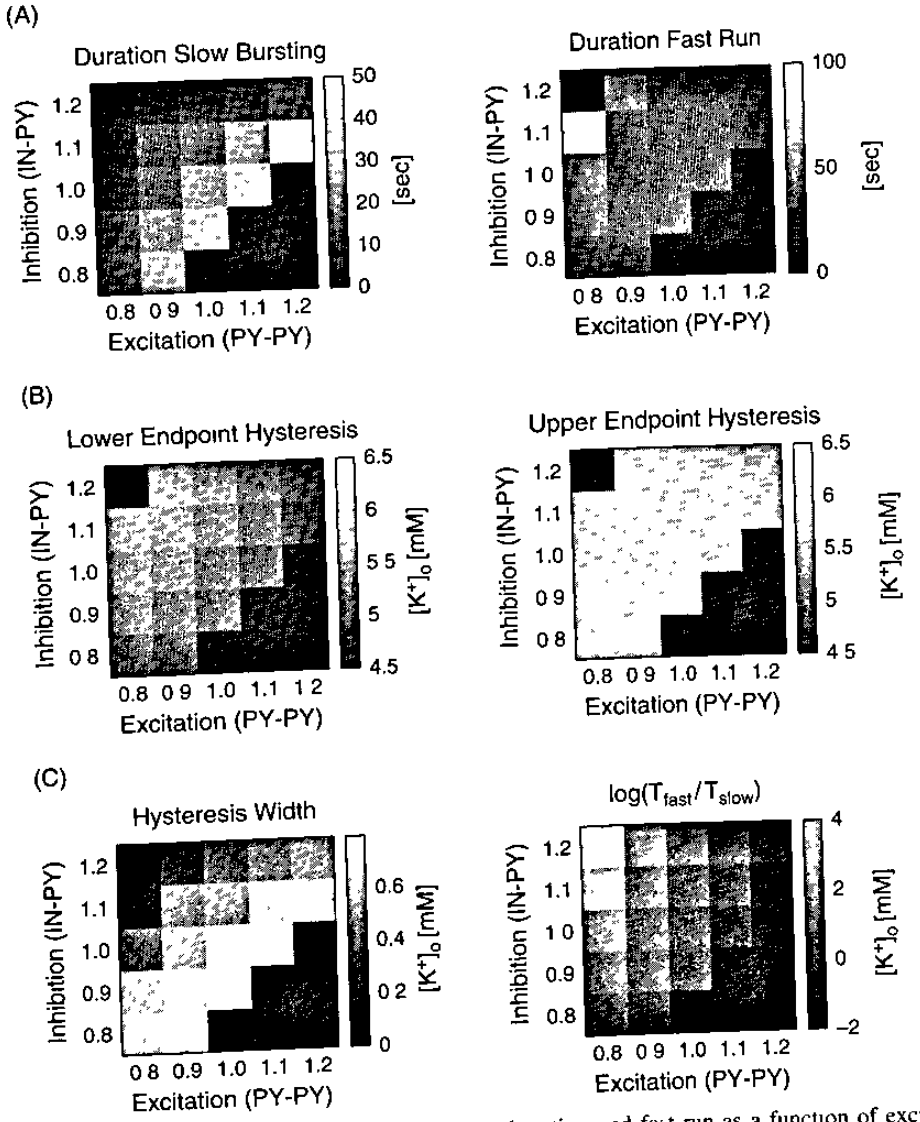

FIGURE 26.6 Quantification of periodic slow transitions between slow bursting and fast run as a function of excitatory and inhibitory coupling Balanced excitation and inhibition causes alternating epochs of slow bursting and fast run (A) Left: duration of epochs of slow bursting. Right: duration of epochs of fast run Values determined from simulation of 400 s of activity. (B) Lower (left) and upper (right) endpoint of hysteresis. (C) Width of hysteresis (right) and logarithmic ratio of duration of fast run and slow bursting (right) as a function of synaptic excitation and inhibition. Top left corner corresponds to regime with exclusive fast run, whereas bottom right corner denotes the regime with exclusive slow bursting. Adapted from Frohlich et al. (2006), with permission. Copyright 2006 Society for Neuroscience.

of strongly unbalanced excitation and inhibition, no state transitions were found. For strong excitation and weak inhibition, bursting followed by silence occurred. Quite the opposite was observed for weak excitation and strong inhibition; the network displayed activity similar to fast run without exhibiting any slow state transitions and never returned to the silent state. In summary, balanced excitation and inhibition was found to be crucial for the occurrence of patterned oscillatory network activity in network models of cortical circuits with potassium dynamics.

The resulting slow state transitions are an interesting phenomenon for a series of reasons. First, the model exhibits slow dynamics in absence of any process with an explicit slow time-scale. The transitions occur on a time-scale of seconds (larger network with local synaptic connectivity shown in Figure 26.7), whereas the slowest processes in the

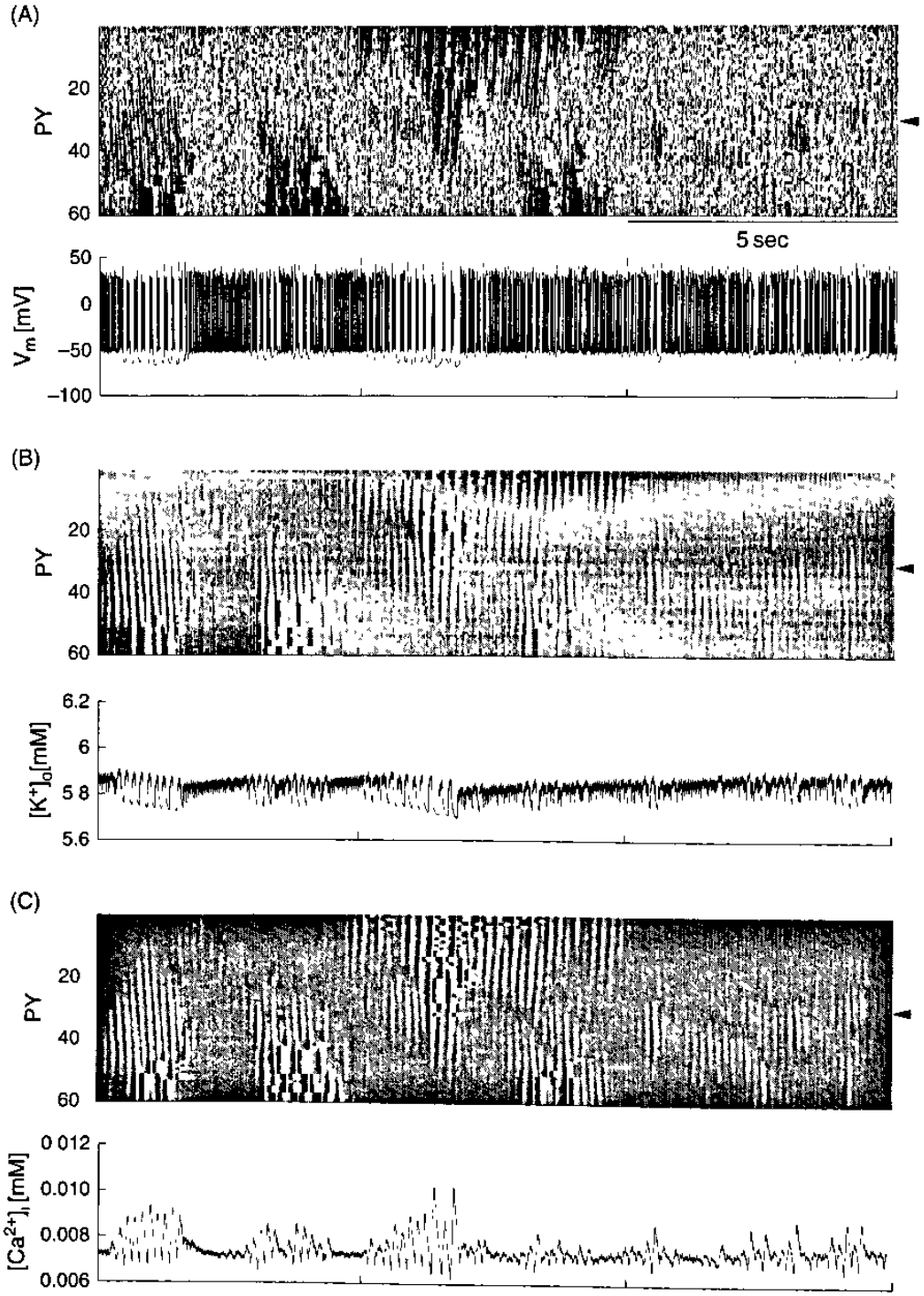

FIGURE 26.7 Large network (60 PY cells and 15 INs) with local synaptic connectivity. (A) PY cell activity as a function of time (top panel). Time-course of V_m for PY 30 (bottom panel, arrow in top panel). Cells switched between bursting and fast run as in the case of the small network. Due to the local synaptic connectivity, the activity pattern exhibited complex spatial structure. (B) $[K+]_o$ in extracellular compartments surrounding PY cells as a function of time (top panel). Time-course of $[K+]_o$ for PY 30 (bottom panel, arrow in top panel). (C) Intracellular calcium $[Ca^{2+}]_i$ in PY cells as a function of time. Time-course of $[Ca^{2+}]_i$ for PY 30 (bottom panel, arrow in top panel). From Frohlich et al. (2006), with permission. Copyright 2006 Society for Neuroscience

model have time-constants of at most a few hundred milliseconds. Rather, the slow dynamics emerge from the interaction of fast processes increasing and decreasing $[K+]_o$. Very slow evolution of $[K+]_o$ is the net effect of this push and pull dynamics close to the equilibrium (where the $[K+]_o$ gradient is zero). Second, the model predicts specific $[K+]_o$ gradients during the two oscillatory phases: positive in case of fast run and negative in case of slow bursting. This matches the experimental *in vivo* (Sypert and Ward, 1974) and *in vitro* (Jensen and Yaari, 1997) finding of increasing and decreasing $[K+]_o$ during tonic and clonic components of seizures. Third, these slow transitions closely resemble the patterned activity during electrographic seizure in cat *in vivo* (see Figure 26.1) and clinical seizures in patients suffering from the Lennox-Gastaut syndrome. The mechanism underlying this patterning of oscillatory firing has so far remained elusive. Our network model including extracellular potassium dynamics provides a novel mechanistic explanation for these slow state transitions.

FAILURE OF K^+ REGULATORY SYSTEM LEADS TO PAROXYSMAL OSCILLATIONS

The previous section established that extracellular potassium concentration dynamics can explain slow state transitions between two distinct oscillatory firing modes resembling neocortical paroxysmal activity *in vivo*. Experimental evidence suggests that, in certain epileptic brains, the potassium regulatory system exhibits deficits. Post-traumatic hippocampal glia cells failed to maintain K^+ homeostasis in the extracellular space (D'Ambrosio et al., 1999) leading to increased $[K+]_o$ and afterdischarges during stimulation *in vitro* (but see Santhakumar et al., 2003). Hippocampal tissue from human patients with temporal lobe epilepsy exhibited impairment of glial inward-rectifying K^+-channels responsible for K^+ uptake (Hinterkeuser et al., 2000; Kivi et al., 2000).

Here, the computational model of a cortical circuit with extracellular potassium dynamics is used to test the hypothesis that such deficits in the mechanisms responsible for $[K+]_o$ homeostasis can lead to paroxysmal oscillations. Specifically, the following two cases are investigated: (1) blocking of potassium pumps and (2) blocking of glial cell buffering.

Role of K^+ pump

In the case of a single model PY cell surrounded by an extracellular compartment endowed with glial buffering of excess potassium but no K^+ pump for active reuptake, random external synaptic input led to bursting at a range of slow frequencies accompanied by a moderate increase in $[K+]_o$ (Figure 26.8A). In a network (100 PYs and 20 INs), initial random firing increased in frequency for cells which lacked a functioning K^+ pump. As a result, K^+ further increased, effectively mediating a positive feedback loop. After a few seconds, the network started to burst at slow frequency with neighboring groups of neurons bursting in synchrony (Figure 26.8B). These bursting oscillations were persistent even after removal of the external input. Hence, the potassium regulation system found a new equilibrium state in the absence of potassium pumps. $[K+]_o$ converged to an elevated value for which any further increase in $[K+]_o$ by bursting was balanced by glial potassium buffering.

Role of K^+ buffering

In the absence of glial buffering, a single model neuron fired bursts with spike inactivation and pronounced after-hyperpolarization (see Figure 26.8C). The long depolarized phase during the burst allowed substantial potassium outflow, which rapidly accumulated in the extracellular compartment due to the absence of glial buffering. The resulting depolarization of the potassium reversal potential weakened the calcium-activated potassium current, which mediates burst termination. Eventually, the cell became locked in the depolarized state where no more spiking occurred due to substantial inactivation of the transient voltage-gated sodium channels and no more hyperpolarization occurred since the calcium-activated potassium current was too weak to repolarize the neuron.

In the network case, cells without glial buffering in their extracellular space exhibited a transient phase of slow bursting oscillation before $[K+]_o$ was sufficiently elevated for the cells to switch to the depolarized state with spike-inactivation (see Figure 26.8D, top panel). Adding lateral diffusion of potassium changed the qualitative nature of the dynamics (see Figure 26.8D, middle and bottom panel). The potassium accumulating in the extracellular compartments with no glial buffering diffused into compartments with intact glial buffering and therefore lower $[K+]_o$. As a consequence, the whole network exhibited slow bursting, even in the absence of external input. No more long-lasting depolarization was observed. In summary, impairment of the glial buffering system had a dramatic effect on the network dynamics and can explain paroxysmal bursting.

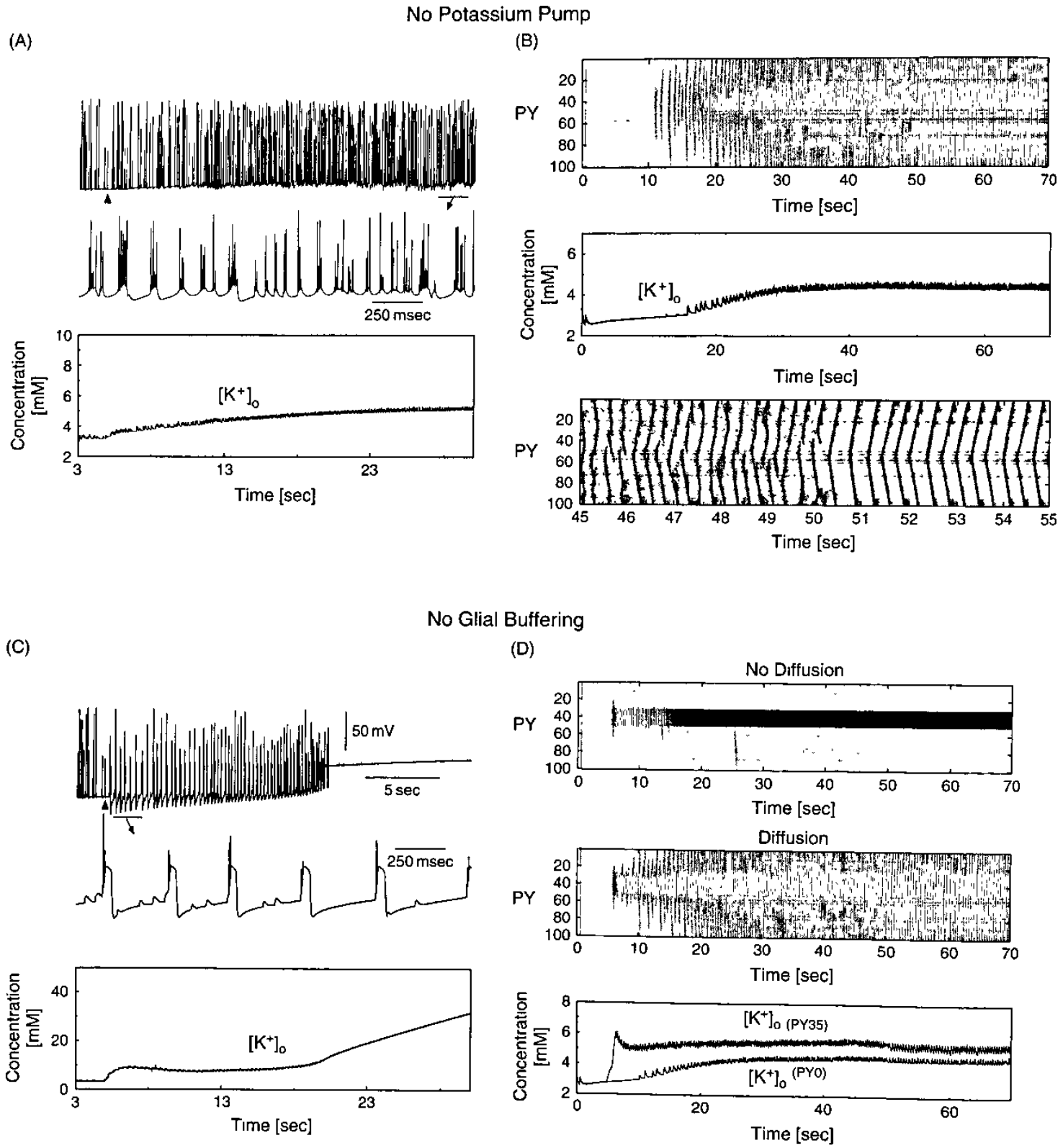

FIGURE 26.8 Effect of glial buffering and K^+ pump on a neuron activity. (A) Following block of K^+ pump (arrowhead), $[K+]_o$ increased and led to fast bursting in single cell model. (B) Blocking the K^+ pump at t = 5 s led to increase of $[K+]_o$ and bursting. Oscillations continued after removing random external input at t = 50 s. A group of cells with I_h led the network oscillations. (C) Blocking glial K^+ uptake system transformed random firing maintained by random external stimulation into periodic bursting and eventually led to permanent spike inactivation. (D) Glial buffering system was blocked in a group of cells (no. 30–50) at t = 5 s. Top: low-frequency bursting was found in this group and was followed by permanent spike inactivation at about t = 20 s. Middle and bottom: when lateral (between cell) diffusion of K^+ was introduced to the model, the cells outside the group also increased firing. After external random input to the network was removed at t = 50 s, the network displayed periodic oscillations at about 3 Hz. Adapted from Bazhenov et al. (2004), used with permission. Copyright 2004 the American Physiological Society.

TERMINATION OF PAROXYSMAL OSCILLATIONS BY SHIFTING BALANCE OF EXCITATION AND INHIBITION

Little is known about seizure cessation (Timofeev and Steriade, 2004). Although the network model with extracellular potassium dynamics discussed above explains initiation and maintenance of neocortical electrographic seizures characterized by alternating epochs of fast run and slow bursting, little has been said about possible mechanisms leading to termination of patterned paroxysmal oscillations – seizure cessation. Here, two different mechanisms that both cause a shift in balance between synaptic excitation and inhibition resulting in seizure cessation are described. Both mechanisms are based on the previously discussed finding that persistent oscillations only occurred in case of balanced excitation and inhibition. In case of scaled-up excitation without counterbalance by increased inhibition, the model exhibited only a single epoch of slow bursting during which $[K+]_o$ decreased. As a consequence, the network returned to the silent state without a single episode of fast run. Therefore, any activity-dependent mechanism which shifts the balance between excitation and inhibition towards more excitation can potentially terminate the oscillations. To confirm this hypothesis, the network model with extracellular potassium dynamics was refined by adding slow, activity-dependent modulation of synaptic currents.

Synaptic plasticity

In the first case, 'slow synaptic depression' similar to the standard model of use-dependent short-term depression (STD) was used for both the excitatory (recurrent excitation among pyramidal cells) and the inhibitory (inhibition onto pyramidal cells) synaptic conductances (Figure 26.9). However, parameters were different from the STD model. The recovery time-scale was

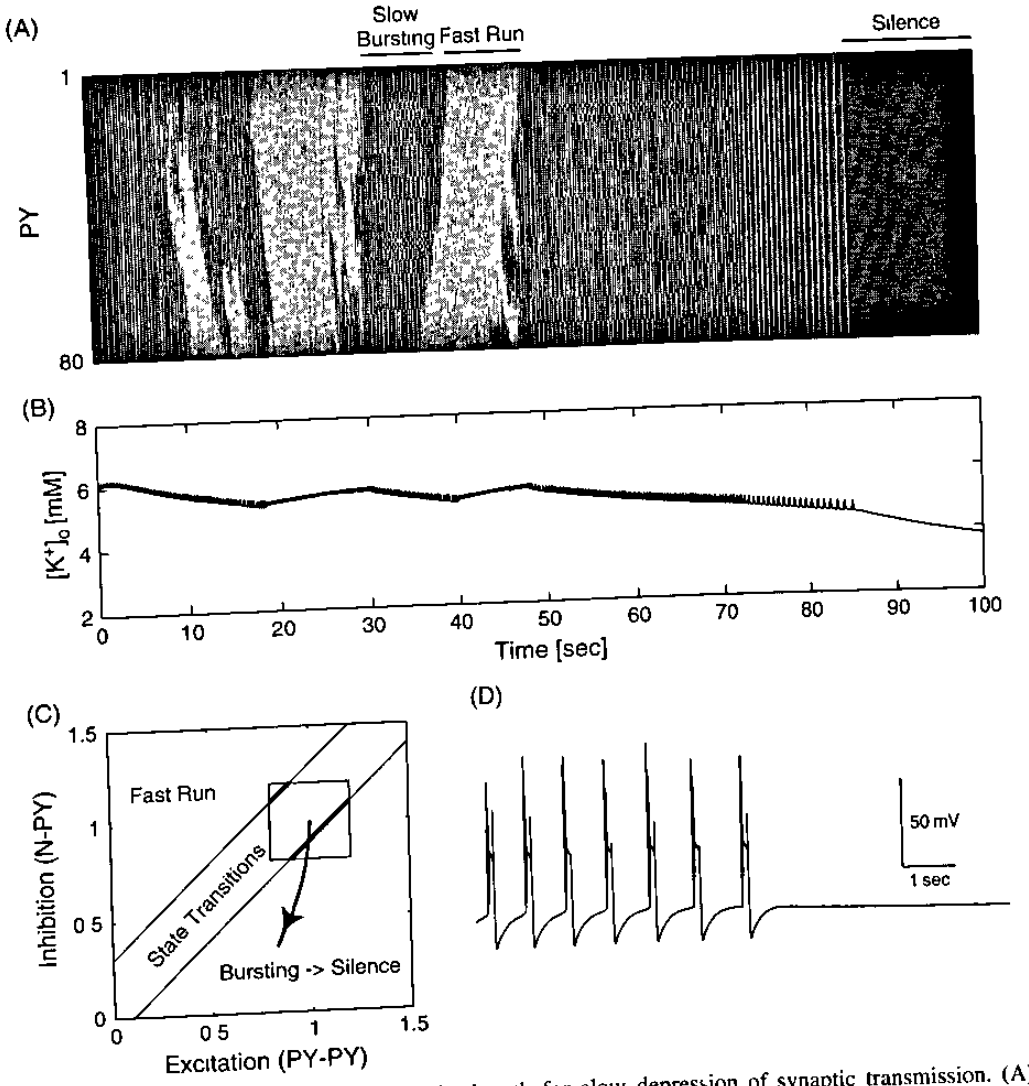

FIGURE 26.9 Patterned cortical network oscillations of finite length for slow depression of synaptic transmission. (A) Activity of all 80 PYs as a function of time. (B) Extracellular potassium concentration time-course (C) Phase-space representation of normalized synaptic coupling strength. Dynamic change in balance between excitation and inhibition (line with arrowhead) Arrowhead indicates direction of time. Diagonal lines delimit the region for which alternating epochs of fast run and slow bursting may occur infinitely The box corresponds to the values of synaptic coupling strengths for which we found persistent oscillations in a small network with the same dynamics (Frohlich et al., 2006). (D) Time-course of membrane voltage before termination of oscillations shows slow bursting.

set to a very slow value such that there was no effective recovery on the time-course of an individual seizure ($\tau = 1000$ s) and the fraction of synaptic resources used per presynaptic action potential was several magnitudes smaller in comparison to STD. As a result, both excitation and inhibition decreased during the paroxysmal oscillatory activity. When the rates were chosen such that inhibition decreased faster than excitation, a net shift in balance between synaptic excitation and inhibition occurred. In the case of parameters causing a fast divergence from the balanced condition, no epoch of fast run occurred. In the limit, this corresponds to the previously discussed, static case where too strong excitatory coupling would not permit slow state transitions. If, however, the values were chosen such that divergence from the balanced condition occurred at a slower speed, which allowed the occurrence of few slow state transitions before the region of approximately balanced synaptic excitation and inhibition was left, the model exhibited both maintenance of patterned oscillatory activity and termination on a time-scale comparable to the paroxysmal events observed *in vivo*. This shows that a shift in balance between excitation and inhibition permits seizure cessation in the model. However, it is not trivial to match the relatively simple slow depression mechanism in the model with actual physiological processes. Although it is known that plasticity on multiple time-scales occurs during seizure-like events, more experimental evidence is required to fully justify the choice of depression mechanisms and parameters.

Intracellular chloride accumulation

In the model, synaptic inhibition is mediated by receptor channels which activate upon binding to GABA. The inhibitory current is mediated by chloride ions. Chloride has a higher extracellular than intracellular concentration. *In vivo* recordings

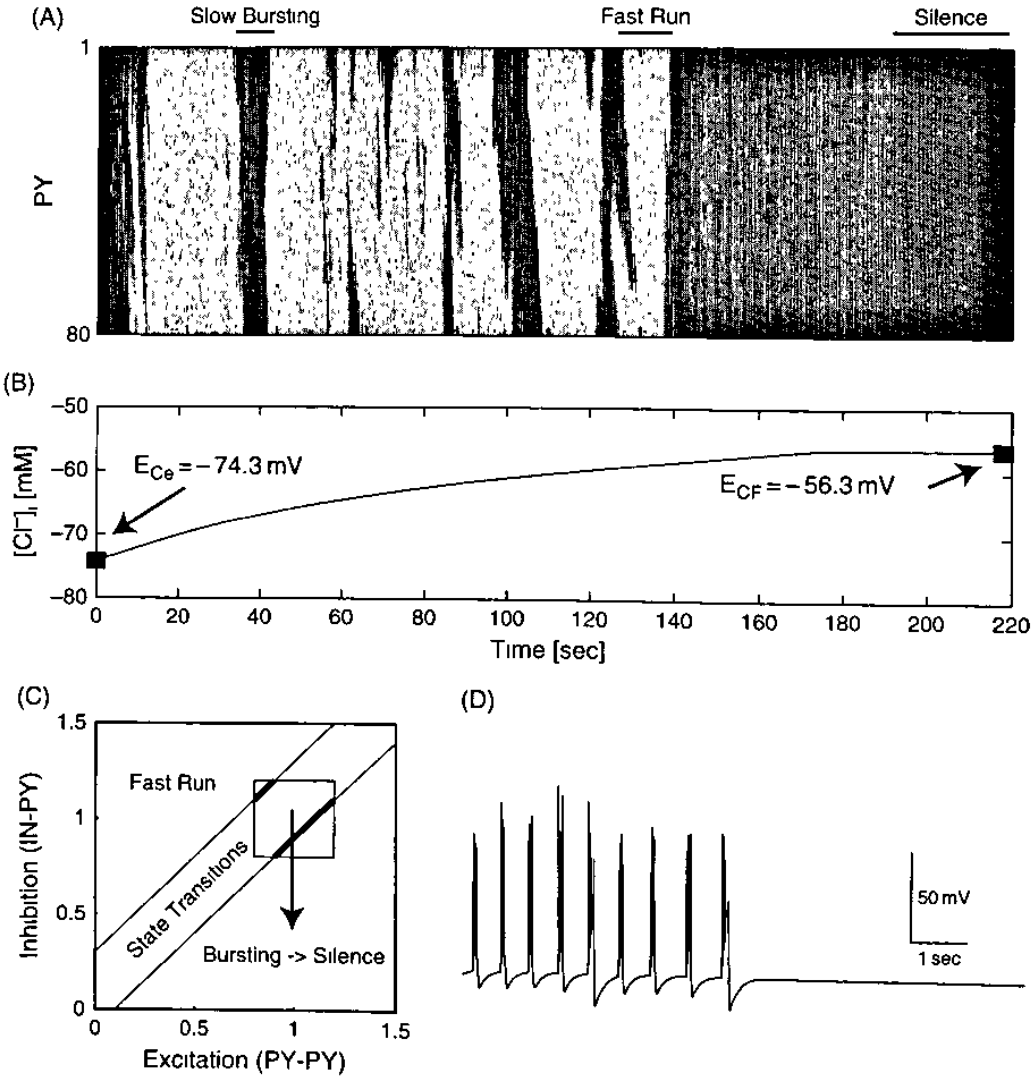

FIGURE 26.10 Patterned cortical network oscillations of finite length for dynamically updated intracellular chloride concentration. (A) Activity of all 80 PYs as a function of time. (B) Intracellular chloride concentration time-course. Corresponding reversal potentials are shown for the onset and the end of oscillations (C) Symbolic phase-space representation of dynamic change in balance between excitation and inhibition (line with arrowhead). Arrowhead indicates direction of time. Diagonal lines delimit the region for which alternating epochs of fast run and slow bursting may occur infinitely. (D) Time-course of membrane voltage before termination of oscillations.

measuring the reversal potential of inhibitory currents showed that the reversal potential for chloride mediated inhibition depolarized from −69.7 to −54.2 mV during seizures (Timofeev et al., 2002). Activity-dependent accumulation of intracellular chloride is the most likely candidate mechanism underlying this shift in reversal potential. In the model, chloride accumulation mediated by inhibitory currents reproduces the depolarization of the reversal potential (Figure 26.10). Similarly to the previous case where synaptic plasticity mediated divergence away from balanced excitation and inhibition, intracellular chloride accumulation caused a selective decrease in inhibition by reduction of the corresponding driving force. This activity-dependent decrease in inhibition caused seizure termination in the model. In summary, an additional state equation, which modeled the intracellular chloride accumulation closely, reproduced the experimentally determined depolarization of the corresponding reversal potential and caused seizure cessation.

CONCLUSION

Over the past decades, computational models of neurons and networks of neurons have provided significant insight into how the nervous system functions. The efforts discussed in this chapter contribute to the relatively young field of mathematical and computational modeling of pathological brain states. The work presented here is focused on the investigation of the mechanism underlying neocortical paroxysmal oscillations. Although an increase in intrinsic excitability via increase in extracellular potassium concentration had been implicated in epileptogenesis for decades, little about the resulting dynamics had been established. Most commonly, increase in $[K+]_o$ has been associated with a positive feedback mechanism eventually leading to depolarization with spike inactivation by some form of global loss of stability (potassium accumulation hypothesis).

We have found that extracellular potassium dynamics explains slow state transitions between two metastable oscillatory states, fast run and slow bursting. Bifurcation analysis has helped to understand the underlying dynamics in terms of the newly discovered bistability between tonic firing and slow bursting in the model cortical neuron. Our potassium model of neocortical epilepsy reproduces the main features of paroxysmal cortical activity characterized by alternating epochs of slow bursting and fast run as observed in human patients with the Lennox-Gastaut syndrome.

We conclude by suggesting that:

1. $[K+]_o$ dynamics mediate slow transitions between SW discharges and fast runs in cortical seizures
2. $[K+]_o$ increases during tonic discharges and decreases during clonic discharges
3. pyramidal cells fire either tonically or in slow bursts depending on $[K+]_o$
4. slow state transitions between tonic and clonic activity occur in conditions of balanced excitation and inhibition
5. a shift in the balance between synaptic excitation and inhibition towards more excitation mediates seizure cessation
6. cortical tonic-clonic seizures end with a clonic epoch. The last prediction has been observed *in vivo* (I. Timofeev, unpublished observation).

The hypotheses derived from our modeling work need to be tested by new experiments to further investigate the role of extracellular potassium dynamics in seizure initiation, maintenance and termination. We hope that these studies will eventually contribute to the development of new clinical methods of prevention and intervention in patients suffering from epilepsy.

ACKNOWLEDGMENT

This study was supported by National Institute on Deafness and Other Communication Disorders, National Institutes of Health (Grant R01 DC006306), Canadian Institutes of Health Research (Grant MOP-37862, MOP-67175) and Natural Science and Engineering Research Council of Canada. I.T. is Canadian Institutes of Health Research scholar.

REFERENCES

Ajmone-Marsan, C. and Ralston, B. (1956). Thalamic control of certain normal and abnormal cortical rhythms. Electroencephalogr Clin Neurophysiol Suppl 8.559–582.

Amzica, F. and Steriade, M. (2000). Neuronal and glial membrane potentials during sleep and paroxysmal oscillations in the neocortex. J Neurosci 20·6648–6665.

Bal, T., von Krosigk, M. and McCormick, D A (1995). Synaptic and membrane mechanisms underlying synchronized oscillations in the ferret lateral geniculate nucleus in vitro. J Physiol 483 (Pt 3):641–663.

Bazhenov, M , Timofeev, I , Steriade, M. and Sejnowski, T.J. (2004). Potassium model for slow (2–3 Hz) in vivo neocortical paroxysmal oscillations. J Neurophysiol 92:1116–1132.

Castro-Alamancos, M.A. (1999). Neocortical synchronized oscillations induced by thalamic disinhibition in vivo. J Neurosci 19:RC27.

D'Ambrosio, R , Maris, D O , Grady, M.S., Winn, H R and Janigro, D. (1999). Impaired K(+) homeostasis and altered electrophysiological properties of post-traumatic hippocampal glia. J Neurosci 19:8152–8162.

Destexhe, A., Mainen, Z.F. and Sejnowski, T.J. (1994). Synthesis of models for excitable membranes, synaptic transmission and neuromodulation using a common kinetic formalism. J Comput Neurosci 1:195–230.

Dichter, M.A., Herman, C.J. and Selzer, M. (1972). Silent cells during interictal discharges and seizures in hippocampal penicillin foci. Evidence for the role of extracellular K+ in the transition from the interictal state to seizures. Brain Res 48:173–183.

Ermentrout, B. (1996). Type I membranes, phase resetting curves, and synchrony. Neural Comput 8 979–1001.

Fertziger, A P. and Ranck, J.B. Jr (1970). Potassium accumulation in interstitial space during epileptiform seizures. Exp Neurol 26:571–585.

Frohlich, F. and Bazhenov, M. (2006). Coexistence of tonic firing and bursting in cortical neurons. Phys Rev E Stat Nonlin Soft Matter Phys 74.

Frohlich, F., Bazhenov, M., Timofeev, I., Steriade, M. and Sejnowski, T.J (2006). Slow state transitions of sustained neural oscillations by activity-dependent modulation of intrinsic excitability. J Neurosci 26.6153–6162.

Futamachi, K.J., Mutani, R. and Prince, D A (1974). Potassium activity in rabbit cortex. Brain Res 75:5–25.

Grossman, R G. and Hampton, T. (1968). Depolarization of cortical glial cells during electrocortical activity. Brain Res 11:316–324.

Heinemann, U. and Lux, H.D. (1977). Ceiling of stimulus induced rises in extracellular potassium concentration in the cerebral cortex of cat. Brain Res 120:231–249.

Heinemann, U., Lux, H.D. and Gutnick, M J. (1977). Extracellular free calcium and potassium during paroxsmal activity in the cerebral cortex of the cat. Exp Brain Res 27:237–243.

Hinterkeuser, S., Schroder, W., Hager, G. et al (2000) Astrocytes in the hippocampus of patients with temporal lobe epilepsy display changes in potassium conductances Eur J Neurosci 12:2087–2096.

Hotson, J.R., Sypert, G.W. and Ward, A.A. Jr (1973) Extracellular potassium concentration changes during propagated seizures in neocortex. Exp Neurol 38.20–26.

Izhikevich, E.M. (2007). *Dynamical systems in neuroscience: the geometry of excitability and bursting*. MIT Press: Cambridge MA.

Jensen, M.S. and Yaari, Y. (1997) Role of intrinsic burst firing, potassium accumulation, and electrical coupling in the elevated potassium model of hippocampal epilepsy. J Neurophysiol 77:1224–1233

Jensen, M.S., Azouz, R. and Yaari, Y. (1994). Variant firing patterns in rat hippocampal pyramidal cells modulated by extracellular potassium. J Neurophysiol 71 831–839.

Kivi, A., Lehmann, T.N., Kovacs, R. et al (2000) Effects of barium on stimulus-induced rises of [K+]o in human epileptic non-sclerotic and sclerotic hippocampal area CA1. Eur J Neurosci 12.2039–2048.

Lothman, E., Lamanna, J., Cordingley, G., Rosenthal, M. and Somjen, G. (1975). Responses of electrical potential, potassium levels, and oxidative metabolic activity of the cerebral neocortex of cats Brain Res 88:15–36.

Lux, H D. and Neher, E. (1973). The equilibration time course of (K +) 0 in cat cortex. Exp Brain Res 17:190–205.

Mainen, Z.F. and Sejnowski, T.J. (1996). Influence of dendritic structure on firing pattern in model neocortical neurons. Nature 382:363–366.

Markand, O.N. (2003). Lennox-Gastaut syndrome (childhood epileptic encephalopathy). J Clin Neurophysiol 20:426–441.

Markram, H., Pikus, D., Gupta, A and Tsodyks, M. (1998). Potential for multiple mechanisms, phenomena and algorithms for synaptic plasticity at single synapses. Neuropharmacology 37 489–500.

Moody, W J , Futamachi, K.J. and Prince, D.A. (1974). Extracellular potassium activity during epileptogenesis. Exp Neurol 42:248–263.

Niedermeyer, E. (1999a). Abnormal EEG patterns: epileptic and paroxysmal. In Electroencephalography: basic principles, clinical applications, and related fields (E. Niedermeyer and F. Lopes de Silva F, eds), pp. 235–260 Williams & Wilkins, Baltimore.

Niedermeyer, E. (1999b) Epileptic seizure disorders. In: In: Electroencephalography: basic principles, clinical applications, and related fields (E Niedermeyer and F. Lopes de Silva F, eds), pp. 476–585. Williams & Wilkins, Baltimore.

Niedermeyer, E. (2002). Lennox-Gastaut syndrome. Clinical description and diagnosis. Adv Exp Med Biol 497:61–75.

Pinault, D., Leresche, N., Charpier, S. et al. (1998). Intracellular recordings in thalamic neurones during spontaneous spike and wave discharges in rats with absence epilepsy. J Physiol 509 (Pt 2):449–456.

Prince, D.A., Lux, H.D. and Neher, E. (1973). Measurement of extracellular potassium activity in cat cortex. Brain Res 50:489–495.

Rinzel, J. and Ermentrout, B. (1989). Analysis of neural excitability and oscillations. In: Methods in neuronal modeling (C. Koch and I. Segev, eds). MIT Press, Cambridge.

Rutecki, P.A., Lebeda, F.J and Johnston, D. (1985) Epileptiform activity induced by changes in extracellular potassium in hippocampus. J Neurophysiol 54 1363–1374.

Santhakumar, V., Voipio, J., Kaila, K. and Soltesz, I. (2003). Post-traumatic hyperexcitability is not caused by impaired buffering of extracellular potassium. J Neurosci 23.5865–5876.

Singer, W. and Lux, H D. (1973). Presynaptic depolarization and extracellular potassium in the cat lateral geniculate nucleus. Brain Res 64:17–33.

Singer, W. and Lux, H D. (1975). Extracellular potassium gradients and visual receptive fields in the cat striate cortex. Brain Res 96:378–383.

Stafstrom, C.E. (2005). Neurons do the wave (and the spike!) during neocortical seizures. Epilepsy Curr 5:69–71.

Steriade, M. (1974). Interneuronal epileptic discharges related to spike-and-wave cortical seizures in behaving monkeys. Electroencephalogr Clin Neurophysiol 37.247–263.

Steriade, M. (2003). Neuronal substrates of sleep and epilepsy. Cambridge University Press, Cambridge.

Steriade, M. and Contreras, D. (1995). Relations between cortical and thalamic cellular events during transition from sleep patterns to paroxysmal activity. J Neurosci 15.623–642

Steriade, M. and Contreras, D. (1998). Spike-wave complexes and fast components of cortically generated seizures. I. Role of neocortex and thalamus. J Neurophysiol 80:1439–1455.

Steriade, M and Timofeev, I. (2001). Corticothalamic operations through prevalent inhibition of thalamocortical neurons. Thalamus related syst 1:225–236.

Steriade, M , Amzica, F., Neckelmann, D. and Timofeev, I. (1998). Spike-wave complexes and fast components of cortically generated seizures. II Extra- and intracellular patterns. J Neurophysiol 80:1456–1479.

Sypert, G.W. and Ward, A.A. Jr (1971). Unidentified neuroglia potentials during propagated seizures in neocortex. Exp Neurol 33·239–255.

Sypert, G W. and Ward, A.A. Jr (1974). Changes in extracellular potassium activity during neocortical propagated seizures. Exp Neurol 45.19–41.

Timofeev, I. and Steriade, M. (2004). Neocortical seizures· initiation, development and cessation. Neuroscience 123:299–336

Timofeev, I., Grenier, F. and Steriade, M. (1998). Spike-wave complexes and fast components of cortically generated seizures. IV. Paroxysmal fast runs in cortical and thalamic neurons J Neurophysiol 80:1495–1513.

Timofeev, I., Grenier, F., Bazhenov, M., Sejnowski, T.J. and Steriade, M. (2000). Origin of slow cortical oscillations in deafferented cortical slabs. Cereb Cortex 10·1185–1199.

Timofeev, I., Grenier, F. and Steriade, M. (2002). The role of chloride-dependent inhibition and the activity of fast-spiking neurons during cortical spike-wave electrographic seizures. Neuroscience 114:1115–1132.

Tsodyks, M.V. and Markram, H. (1997) The neural code between neocortical pyramidal neurons depends on neurotransmitter release probability. Proc Natl Acad Sci USA 94:719–723

Yaari, Y., Konnerth, A. and Heinemann, U. (1986). Nonsynaptic epileptogenesis in the mammalian hippocampus in vitro. II. Role of extracellular potassium. J Neurophysiol 56·424–438